Acta Crystallographica Section F
Structural Biology and Crystallization Communications
ISSN 1744-3091

Inducible production of recombinant human Flt3 ectodomain variants in mammalian cells and preliminary crystallographic analysis of Flt3 ligand–receptor complexes

Kenneth Verstraete,[a] Bert Remmerie,[a] Jonathan Elegheert,[a] Beatrice Lintermans,[b] Guy Haegeman,[b] Peter Vanhoenacker,[b] Kathleen Van Craenenbroeck[b] and Savvas N. Savvides[a]*

[a]Unit for Structural Biology, Laboratory for Protein Biochemistry and Biomolecular Engineering (L-ProBE), Ghent University, 9000 Ghent, Belgium, and [b]Laboratory of Eukaryotic Gene Expression and Signal Transduction (LEGEST), Ghent University, 9000 Ghent, Belgium

Correspondence e-mail: savvas.savvides@ugent.be

Received 29 December 2010
Accepted 25 January 2011

The extracellular complex between the haematopoietic receptor Flt3 and its cytokine ligand (FL) is the cornerstone of signalling cascades that are central to early haematopoiesis and the immune system. Here, efficient protocols for the production of two ectodomain variants of human Flt3 receptor, $Flt3_{D1–D5}$ and $Flt3_{D1–D4}$, for structural studies are reported based on tetracycline-inducible stable cell lines in HEK293S cells deficient in *N*-acetylglycosaminyltransferase I ($GnTI^{-/-}$) that can secrete the target proteins with limited and homogeneous N-linked glycosylation to milligram amounts. The ensuing preparative purification of Flt3 receptor–ligand complexes yielded monodisperse complex preparations that were amenable to crystallization. Crystals of the $Flt3_{D1–D4}$–FL and $Flt3_{D1–D5}$–FL complexes diffracted to 4.3 and 7.8 Å resolution, respectively, and exhibited variable diffraction quality even within the same crystal. The resulting data led to the successful structure determination of $Flt3_{D1–D4}$–FL *via* a combination of molecular-replacement and density-modification protocols exploiting the noncrystallographic symmetry and high solvent content of the crystals.

1. Introduction

The Fms-like tyrosine kinase 3 (Flt3) receptor and its cognate cytokine, termed Flt3 ligand (FL), initiate signalling pathways in haematopoietic stem cells and early haematopoietic progenitors of myeloid and lymphoid origin to develop the pluripotent cellular population of the human haematopoietic and immune systems (Onai *et al.*, 2007; Stirewalt & Radich, 2003; Lyman, James, Zappone *et al.*, 1993; Hannum *et al.*, 1994; Drexler & Quentmeier, 2004; Kikushige *et al.*, 2008; Liu & Nussenzweig, 2010; Parcells *et al.*, 2006). Flt3 receptor is primarily expressed on early haematopoietic progenitors in the bone-marrow environment and is crucially involved in the development and homeostasis of antigen-presenting dendritic cells (Schmid *et al.*, 2010; Waskow *et al.*, 2008; Onai *et al.*, 2007). Injection of exogenous FL leads to a massive expansion of dendritic cells and this has prompted its use in cancer immunotherapy (Fong *et al.*, 2001). On the other hand, overexpression of wild-type or oncogenic forms of the Flt3 receptor and/or FL autocrine signalling loops are associated with various haematologic malignancies (Griffith *et al.*, 2004; Zheng *et al.*, 2004; Kiyoi *et al.*, 1998; Stirewalt & Radich, 2003; Kiyoi & Naoe, 2006; Parcells *et al.*, 2006). Most notably, mutational fingerprints in Flt3 are the predominant prognostic factor in acute myeloid leukaemia (AML; Eklund, 2010) and have rationalized the targeting of Flt3 in a clinical setting (Kindler *et al.*, 2010).

Together with platelet-derived growth factor receptors (PDGFRα/β), colony-stimulating factor 1 receptor (CSF-1R) and KIT, Flt3 is a member of the type III receptor tyrosine kinase (RTKIII) family (Grassot *et al.*, 2006). As such, Flt3 has been predicted to exhibit a modular structure featuring an extracellular segment with five immunoglobulin (Ig)-like domains (residues 27–543), a single transmembrane helix (TM; residues 544–563), a cytoplasmic juxtamembrane domain (JM; residues 572–603) and an intracellular kinase module (residues 604–958) (Lyman, James,

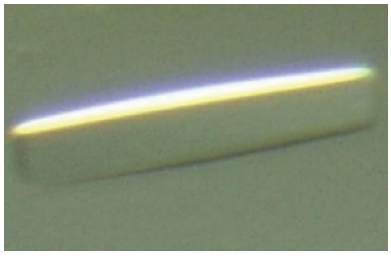

Zappone *et al.*, 1993; Maroc *et al.*, 1993). A fully functional Flt3 isoform that lacks the fifth Ig domain has been identified in mice (Lavagna *et al.*, 1995).

FL is a noncovalently linked dimeric four-helical bundle cytokine that is structurally homologous to stem cell factor (SCF) and colony-stimulating factor 1 (CSF-1), which are the ligands of KIT and CSF-1R, respectively (Lyman, James, Vanden Bos *et al.*, 1993; Hannum *et al.*, 1994; Savvides *et al.*, 2000). Several FL splice variants have been identified (McClanahan *et al.*, 1996; Lyman *et al.*, 1995) leading to biologically active membrane-bound or soluble forms of FL (Escobar *et al.*, 1995), which activate the receptor by ligand-induced dimerization (Kiyoi *et al.*, 2002). Despite the staggering body of biomedical literature on the physiological and clinical importance of the Flt3–FL complex, the structural basis of the Flt3 extracellular assembly has remained uncharacterized. Here, we report protocols for the efficient production of Flt3 ectodomain variants and the crystallization of their complexes with FL for structural studies.

2. Experimental procedures

2.1. Expression constructs

A cDNA clone (Image ID 5272266) encoding the full-length human Flt3 receptor was purchased from IMAGENES. PCR fragments encoding residues 1–540, 27–540 and 27–437 were gel-purified (Qiagen, catalogue No. 28704) and subcloned into the pCR2.1-TOPO vector (Invitrogen, catalogue No. KNM4500-01). Mammalian expression constructs were generated in the pHLsec (Aricescu *et al.*, 2006) and pcDNA4/TO (Invitrogen, catalogue No. V1020-20) vectors by restriction site-dependent cloning. Modified versions of these vectors contained the Cystatine S (Barash *et al.*, 2002) or Mu (Aricescu *et al.*, 2006) secretion signal at their multicloning site. All expression constructs included a C-terminal hexahistine tag. Plasmid DNA was propagated in *Escherichia coli* TOP10 cells (Invitrogen, catalogue No. C4040-50) and purified by chromatography (Qiagen, catalogue No. 12145). PCR was performed using Easy-A polymerase (Stratagene, catalogue No. 600400). Restriction enzymes were purchased from New England Biolabs. Inserts were ligated into the expression vectors using the LigaFast ligation system (Promega, catalogue No. M8221). The final expression constructs were sequence-verified (Cogenics, Meylan, France) and matched the human Flt3 reference sequence in the NCBI database (NP_004110.2).

2.2. Transient expression of Flt3 in HEK293 cells

The human embryonic kidney cell lines HEK293T (ATCC No. CRL-1573) and HEK293S GnTI$^{-/-}$ TetR (Reeves *et al.*, 2002) were grown in DMEM/F12 medium (GIBCO/Invitrogen, catalogue No. 32500–043) supplemented with 10% heat-inactivated foetal calf serum (FCS; Sigma, catalogue No. F7524), 3 m*M* L-glutamine (Sigma, catalogue No. G3126), 10^6 units l^{-1} of penicillin G (Sigma, catalogue No. P7794) and 1 g l^{-1} streptomycin (Sigma, catalogue No. S9137) in a 5% CO_2 atmosphere at 310 K. Small-scale transient expression tests were performed in six-well tissue-culture plates (Corning, catalogue No. 3506) as described by Aricescu *et al.* (2006). The medium of confluently grown cells was replaced with serum-free medium containing 5 µ*M* kifunensine (Toronto Research Chemicals, catalogue No. K450000) and purified plasmid DNA mixed with 25 kDa branched polyethyleneimine (Sigma, catalogue No. 408727) was added. Transfected cells were allowed to express the recombinant protein for 5 d and samples were prepared by mixing the medium with half a volume of Laemmli buffer containing β-mercaptoethanol. Recombinant proteins in the conditioned medium were separated by SDS–PAGE (15% gel), followed by Western blot analysis using an HRP-coupled antibody directed against the C-terminal His tag (Invitrogen, catalogue No. R931-25). Femto Luminol (Thermo Scientific, catalogue No. 34095) was used as the chemiluminescent substrate. Large-scale expression experiments in HEK293T cells were performed in roller bottles (GBO, catalogue No. 681070).

2.3. Tetracycline-inducible stable HEK293S GnTI$^{-/-}$ cell lines secreting recombinant Flt3 ectodomains

pcDNA4/TO expression contructs (containing the Mu secretion signal) were linearized in a non-essential region using the *Sap*I restriction enzyme (NEB) and the DNA was repurified using QIAquick Spin columns (Qiagen, catalogue No. 28104). 4 h prior to transfection, the medium of 50% confluent HEK293S GnTI$^{-/-}$ TetR cells grown in a 75 cm^2 tissue-culture flask (Corning, catalogue No. 430725) was replaced with fresh medium. Cells were transfected according to the calcium phosphate method using 30 µg linearized DNA per flask. 4 h post-transfection the medium was again replaced with fresh medium. After 24 h the transfected cells were detached with trypsin/EDTA and diluted in three 175 cm^2 flasks at different dilutions under selective pressure (200 µg ml^{-1} Zeocin, Invivogen, catalogue No. ant-zn-1). Subsequently, the medium was refreshed every 3–4 d until foci appeared (after 2–3 weeks). Ten foci were isolated using filter papers soaked with trypsin/EDTA, transferred to 24-well tissue-culture plates and subsequently expanded to 175 cm^2 flasks (Greiner Bio-One, catalogue No. 660160). Concomitantly, the clones were tested for protein expression in six-well format. To induce expression, the growth medium of confluently grown cells was replaced with serum-free medium supplemented with 2 µg ml^{-1} tetracycline (Duchefa, catalogue No. T0150) and 5 m*M* sodium butyrate (Sigma, catalogue No. 303410). The expression levels of the clones were compared by Western blot analysis. The most strongly expressing clones were prepared for long-term storage at 193 K using a mixture of 50% cells in DMEM and 50% freezing solution [80% FCS and 20% DMSO (Sigma, catalogue No. D2650)]. For large-scale expression experiments, the medium of 50 × 175 cm^2 tissue-culture flasks was used. The medium was collected 5 d post-induction and clarified from cell debris by centrifugation; it was finally stored at 253 K until further use.

2.4. Selenomethionine labelling of recombinant Flt3$_{D1–D4}$

Cells were grown using the conditions described in §2.2. Prior to induction, the cells were washed once with phosphate-buffered saline (PBS) in order to remove most of the residual methionine. The growth medium was replaced with serum-free DMEM medium devoid of methionine (MP Biomedicals, catalogue No. 091642254) but supplemented with 30 mg l^{-1} selenomethionine (Acros Organics, catalogue No. 259960010). We observed a significant reduction in protein expression compared with our standard protocols, which we attribute to increased levels of cell death owing to the toxicity of selenomethione.

2.5. Protein purification

Defrosted medium (2.5 l) was filtered through a 0.22 µm bottle-top filter (Corning, catalogue No. 431174) and without further additions was loaded overnight onto a Talon Superflow column (Clontech, catalogue No. 635507) with a bed volume of 20 ml connected to an ÄKTApurifier (GE Healthcare) system and equilibrated with 300 m*M* NaCl, 50 m*M* NaH_2PO_4 pH 7.2 at a flow rate of 5 ml min^{-1}. After loading, the column was washed with equilibration buffer

containing 5 m*M* imidazole and the protein was eluted with buffer containing 200 m*M* imidazole. EDTA (1 m*M*) and protease inhibitors (Roche, catalogue No. 11873580001) were added to the protein solution (~30 ml). The protein was then concentrated to 1 ml using a Vivaspin concentrator with a molecular-weight cutoff of 10 kDa (Sartorius, catalogue No. VS15RH02)

Subsequently, the partially purified recombinant Flt3 was injected onto a Superdex 200 column (GE Healthcare, catalogue No. 17-1069-01) with 150 m*M* NaCl, 10 m*M* HEPES pH 7.2 as running buffer. The fractions corresponding to recombinant Flt3 were pooled and concentrated to 1 ml using a Vivaspin concentrator (Sartorius, catalogue No. VS0404). As a final polishing step, the protein solution was diluted fivefold with 20 m*M* Tris–HCl pH 7.0 and loaded onto a MonoQ column (GE Healthcare, catalogue No. 17-5166-01) equilibrated with 20 m*M* Tris–HCl pH 7.0. The protein was eluted using a linear gradient from 0 to 1 *M* NaCl and collected in fractions of 200 µl; it was stored at 193 K until further use.

2.6. Crystallization of Flt3 ligand–receptor complexes

Flt3 ligand–receptor complexes were formed by mixing excess molar amounts of purified FL (2 × 138 residues, 31.7 kDa; Verstraete *et al.*, 2009) with the purified receptor ectodomains. Protein concentrations were determined by absorbance at 280 nm using a NanoDrop spectrophotometer and calculated extinction coefficients for the recombinant proteins: $\varepsilon_{280}(\mathrm{Flt3_{D1–D5}}) = 76\,205$, $\varepsilon_{280}(\mathrm{Flt3_{D14}}) = 50\,850$ and $\varepsilon_{280}(\mathrm{FL}) = 39\,710\ M^{-1}\ \mathrm{cm}^{-1}$. The complexes were separated from excess FL by gel filtration using a Superdex 200 column equilibrated with 150 m*M* NaCl, 10 m*M* HEPES pH 7.2. Fractions corresponding to the complex were pooled and concentrated using a Vivaspin concentrator (Sartorius, catalogue No. VS0404) to a final concentration of 5 mg ml^{-1}. The concentrated protein solution was aliquoted, flash-frozen in liquid nitrogen and subsequently stored at 193 K until further use.

Initial crystal screening was carried out using the ProPlex (Molecular Dimensions, catalogue No. MD1-38), Crystal Screen Lite (Hampton Research, catalogue No. HR2-128) and PEG/Ion 1 (Hampton Research, catalogue No. HR2-126) screens. Crystallization drops were set up manually at 293 K in 24-well sitting-drop crystallization plates (Hampton Research, catalogue No. HR3-160) by mixing 1 µl reservoir solution (500 µl) with 1 µl protein solution at a concentration of 5 mg ml^{-1}. Crystallization conditions were optimized using chemicals of the highest purity available.

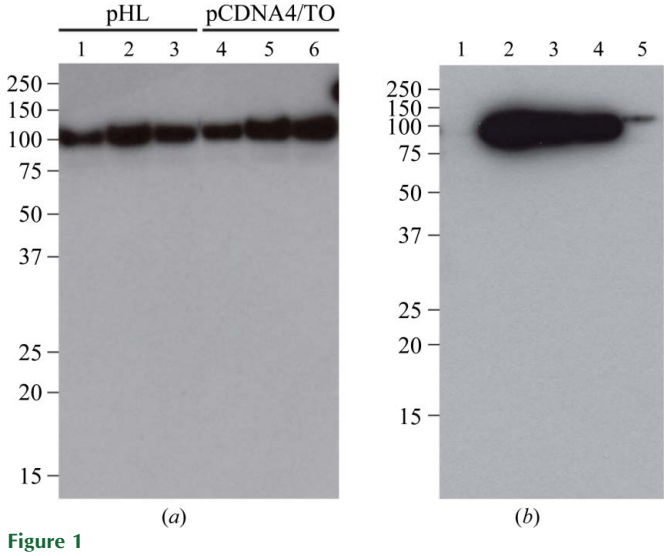

Figure 1
(*a*) Transient expression of $\mathrm{Flt3_{D1–D5}}$ in HEK293T cells. HEK293T cells seeded in six-well plates were transiently transfected with pHL-$\mathrm{Flt3_{D1–D5}}$ (lanes 1–3) and pcDNA4/TO-$\mathrm{Flt3_{D1–D5}}$ (lanes 4–6). 5 d post-transfection, the expression of $\mathrm{Flt3_{D1–D5}}$-His in the medium was analysed by Western blot immunodetection using anti-His-HRP. Lanes 1 and 4, native secretion signal; lanes 2 and 5, Mu secretion signal; lanes 3 and 6, Cystatine S secretion signal. (*b*) Inducible expression in stably tranfected HEK293S GnTI$^{-/-}$ cell lines. A stable HEK293S GnTI$^{-/-}$ $\mathrm{Flt3_{D1–D5}}$ clone was analysed for inducible expression. Cells were seeded in six-well plates and induced for 5 d. Lane 1, serum-free medium (no induction); lane 2, induction with tetracycline and sodium butyrate; lane 3, induction with tetracycline alone; lane 4, induction with the tetracycline analogue doxycycline. As a control, a sample of transiently transfected HEK293T cells was loaded in lane 5. Immunodetection was performed as in (*a*).

2.7. Derivatization of $\mathrm{Flt3_{D1–D4}}$–FL crystals with heavy atoms for phasing

$\mathrm{Flt3_{D1–D4}}$–FL crystals were incubated in stabilization buffer (artificial mother liquor with a 10% higher concentration of precipitant) containing 0.5–5 m*M* of candidate heavy-atom compounds. A variety of Pt^{2+}, Pb^{2+} and Hg^{2+} salts as well as the tantalum cluster Ta_6Br_{12} were tried using different incubation times ranging from 1 min to several hours.

2.8. X-ray data collection and analysis

Single crystals were transferred to a drop of stabilization buffer (artificial mother liquor containing a 10% higher concentration of precipitant) with the use of a nylon loop (Hampton Research) mounted on a SPINE standard cryocap (Molecular Dimensions, catalogue No. MD7-406). The concentration of cryoprotectant was gradually adjusted by adding increasing amounts of stabilizing buffer containing a higher concentration of cryoprotectant to the drop until the desired concentration of cryoprotectant was reached. A 3 min equilibration time was allowed between successive additions. Subsequently, the crystals were flash-frozen in liquid nitrogen and loaded into SPINE/ESRF pucks for storage and transport. Diffraction experiments were conducted on beamlines X06SA (PXI) and X06DA (PXIII) of the Swiss Light Source (Paul Scherrer Institute, Villigen, Switzerland) and ID23-1 of the ESRF (Grenoble, France). All data were integrated and scaled using the *XDS* suite (Kabsch, 2010). Molecular replacement (MR) was performed using *Phaser* (McCoy *et al.*, 2007). MR search models for individual Flt3 extracellular domains were prepared with *CHAINSAW* (Stein, 2008) with the KIT structure (Yuzawa *et al.*, 2007) as a template. Density modification was carried out using *Parrot* (Cowtan, 2010).

3. Results and discussion

3.1. Protein expression and purification

Obtaining sufficient amounts of the Flt3 ectodomain for structural studies proved to be challenging. Our initial strategy was to express the full-length His-tagged Flt3 ectodomain ($\mathrm{Flt3_{D1–D5}}$) by transient expression in HEK293T cells in the presence of kifunensine (Chang *et al.*, 2007; Aricescu *et al.*, 2006) in order to ensure a properly folded recombinant receptor carrying limited N-linked glycans that could be further reduced by treatment with deglycosylating enzymes such as endoglycosidase H (Endo H) for crystallization purposes. However, despite the high quality and stability of the recombinant $\mathrm{Flt3_{D1–D5}}$ obtained *via* this approach, $\mathrm{Flt3_{D1–D5}}$ yields were very low (0.1 mg per litre of culture medium), which posed tremendous hurdles for extensive crystal screening and additional biophysical studies.

Inspired by the work of Barash and coworkers, we exchanged the native Flt3 secretion signal for the Mu secretion signal or the

Cystatine S secretion signal (Barash *et al.*, 2002). Western blot analysis showed that the introduced signal peptides resulted in a moderate increase in the expression level, with the Mu secretion signal showing the largest effect (Fig. 1*a*). After verification by N-terminal sequencing that the leader sequence was correctly processed, the Mu secretion sequence was retained as a general approach to improving the yields of secreted recombinant Flt3. Additional comparisons investigating the expression efficiency of pHL and pcDNA4/TO expression constructs showed similar yields of Flt3, indicating that the presence of SV40-ori (which is present on pcDNA4/TO), which allows episomal replication of the expression plasmid in HEK293T cells, had no obvious effect on expression levels (Fig. 1*a*).

In an effort to further improve our production of recombinant Flt3 (with the Mu secretion signal), we decided to establish stable cell lines in HEK293S GnTI$^{-/-}$ TetR cells. The use of this HEK293 variant offers two major advantages. Firstly, this cell line is devoid of *N*-acetylglucosamyltransferase I (GnTI) activity and is thereby able to express target proteins with limited and homogeneous N-linked glycosylation that is very sensitive to EndoH treatment (Reeves *et al.*, 2002; Chang *et al.*, 2007). Secondly, this cell line is stably transfected with the pcDNA6-TR encoding the tetracycline-responsive repressor, which binds and blocks the promoter in the absence of tetracycline or an analogue such as doxycycline. This allows tetracycline-regulated expression (Reeves *et al.*, 2002; Yao *et al.*, 1998). Inducible expression systems allow the growth of cell cultures under optimal conditions up until the moment of induction, which could have a beneficial effect on the protein yield compared with constitutive expression.

Inducible HEK293S GnTI$^{-/-}$ cell lines were established as described and found to secrete Flt3$_{D1–D5}$ in high amounts upon treatment with tetracycline or doxycycline when compared with transient expression experiments (Fig. 1*b*). The addition of sodium butyrate, a histone deacetylase inhibitor (Monneret, 2005), further boosted the expression levels. Using the same approach, a stable cell line that expressed an Flt3 ectodomain variant lacking the fifth Ig domain (Flt3$_{D1–D4}$) was established. Our rationale for targeting this construct for structural studies was based on the existence of a fully active splice variant of murine Flt3 lacking extracellular domain 5 (Lavagna *et al.*, 1995). Following large-scale expression experiments, the ectodomains were purified from the medium by a combination of metal-affinity chromatography, gel filtration and anion-exchange chromatography. The use of a Talon matrix employing immobilized Co^{2+} in the important first capture step *via* metal-affinity chromatography gave the best results in terms of overall yield and purity. We observed that Ni-Sepharose column matrices consistently suffered from depletion of Ni^{2+} upon passage of clarified culture medium containing the secreted target proteins. The final yields of purified Flt3$_{D1–D5}$ and Flt3$_{D1–D4}$ were ∼2 mg l^{-1} of medium. Flt3 ligand–receptor complexes were formed by the addition of recombinant FL produced in *E. coli* (Verstraete *et al.*, 2009) and were purified by gel-filtration chromatography (Fig. 2) for use in crystallization trials.

The strategy of developing inducible expression in stably transfected HEK293 GnTI$^{-/-}$ cells may be generally applicable for structural studies involving eukaryotic receptor ectodomains that are

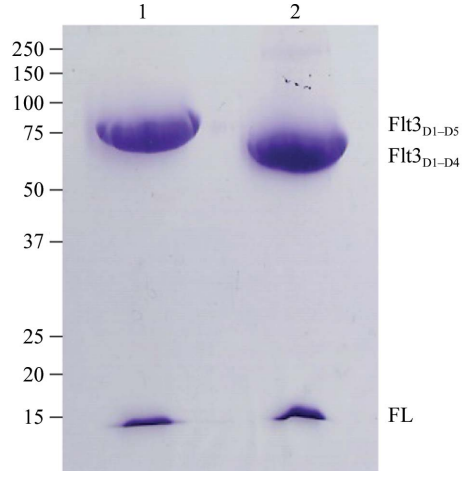

Figure 2
Coomassie-stained SDS–PAGE gel of the purified Flt3–FL complexes. Lane 1, Flt3$_{D1–D5}$–FL; lane 2, Flt3$_{D1–D4}$–FL. The molecular weight of the processed His-tagged Flt3 ectodomains without glycosylation is calculated as 59.7 kDa for Flt3$_{D1–D5}$ (527 residues) and 48.0 kDa for Flt3$_{D1–D4}$ (423 residues). The band at 15 kDa represents denatured FL, which is a homodimer of 31.7 kDa under native conditions.

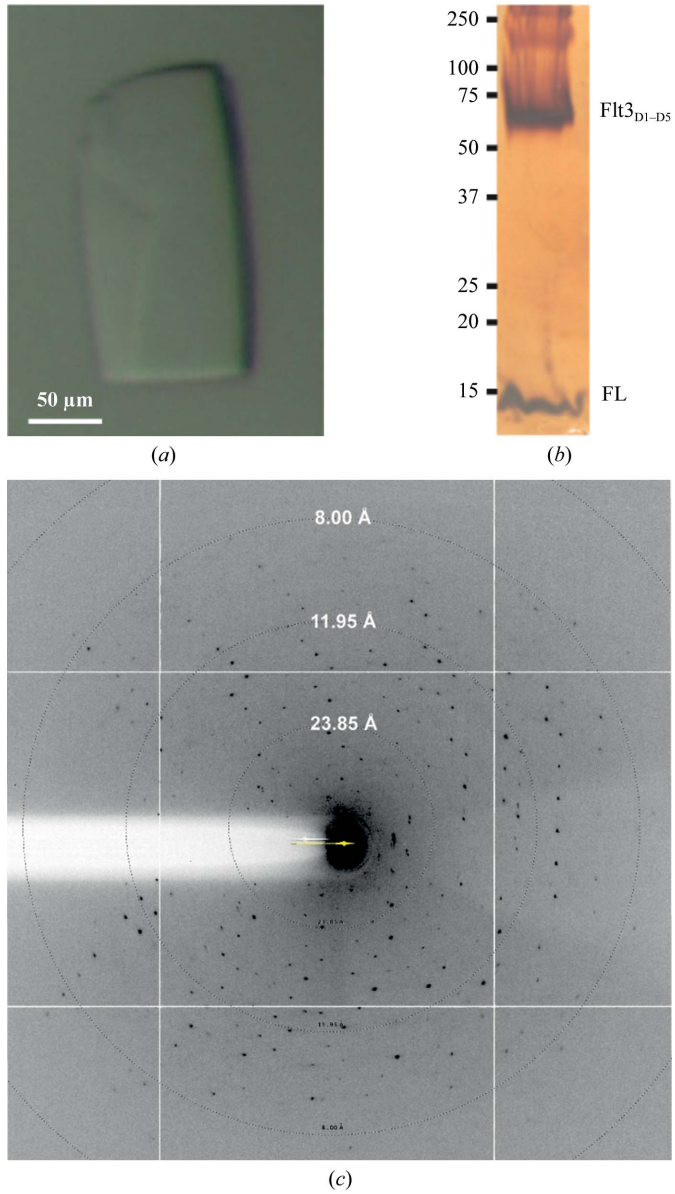

Figure 3
(*a*) Plate-like crystals of the Flt3$_{D1–D5}$–FL complex. (*b*) Silver-stained SDS–PAGE gel confirming the content of dissolved crystals of the Flt3$_{D1-D5}$–FL complex. (*c*) X-ray diffraction image from the Flt3$_{D1–D5}$–FL crystal that led to a complete 7.8 Å data set.

Table 1
X-ray data-collection statistics.

Values in parentheses are for the highest resolution shell.

	$Flt3_{D1–D4}$–FL	$Flt3_{D1–D5}$–FL
Source	ESRF ID23-1	ESRF ID23-1
Wavelength (Å)	0.9714	1.0762
Detector	ADSC Q315R	ADSC Q315R
Resolution (Å)	40.00–4.30 (4.45–4.30)	40.00–7.80 (8.00–7.80)
Space group	$P2_1$	$P2_1$
Unit-cell parameters (Å, °)	a = 103.9, b = 146.3, c = 105.9, β = 109.7	a = 124.7, b = 153.5, c = 133.9, β = 94.6
Wilson B (Å^2)	135	436
Unique reflections	20184 (1942)	5575 (374)
Multiplicity	3.8 (3.8)	3.1 (3.0)
Completeness (%)	98.8 (98.9)	95.3 (90.8)
R_{meas}† (%)	10.8 (75.9)	12.5 (75.9)
Average $I/\sigma(I)$	12.04 (2.08)	8.8 (1.8)
Solvent content‡ (%)	59	71
Matthews coefficient‡ (Å^3 Da^{-1})	3.0	4.2
No. of complexes in asymmetric unit	2	2

† $R_{meas} = \sum_{hkl}[N/(N-1)]^{1/2}\sum_i |I_i(hkl) - \langle I(hkl)\rangle| / \sum_{hkl}\sum_i I_i(hkl)$, where N is the multiplicity, $I_i(hkl)$ is the intensity of the ith measurement of reflection hkl and $\langle I(hkl)\rangle$ is the average value over multiple measurements. ‡ Estimates of solvent content and Matthews coefficients were calculated *via Matthews Probability Calculator* (http://www.ruppweb.org/mattprob/) using the theoretical weight of the complexes without taking N-linked glycosylation into account (Kantardjieff & Rupp, 2003; Matthews, 1968).

difficult to express. Moreover, the high costs associated with low-level transient expression (originating from large-scale plasmid-DNA preparation kits and kifunensine) can thereby be significantly reduced.

3.2. Crystallization of Flt3 complexes and data collection

3.2.1. $Flt3_{D1–D5}$–FL complex. Using commercially available sparse-matrix screens, a dozen hits for the $Flt3_{D1–D5}$–FL complex were identified. These conditions were characterized by the presence of medium-molecular-weight polyethylene glycols (PEG 3350–8000) in the concentration range 10–15% and various salts (chlorides, citrates, phosphates, sulfates, acetates) at 0.1–0.2 *M* as coprecipitant. The pH range varied from 6.5 to 8.5. Crystal optimization coupled with extensive screening *via* X-ray diffraction experiments identified 200 m*M* lithium citrate, 12–14%(*w*/*v*) PEG 3350 and 100 m*M* Tris–HCl pH 7.0 as the best condition. The crystals grew within one week and had a plate-like appearance, with overall dimensions of 0.05 × 0.20 × 0.01–0.20 mm (Figs. 3*a* and 3*b*). However, many crystals were not single or showed obvious physical defects. $Flt3_{D1–D5}$ crystals typically diffracted anisotropically to ∼10 Å resolution using highly collimated synchrotron X-ray beams. Extensive efforts to improve crystal quality using a variety of approaches, including microseeding, crystallization additives and crystal dehydration and annealing protocols (Heras & Martin, 2005), failed to provide consistent improvements in diffraction quality. Furthermore, we were able to grow crystals of the complex after reduction of glycosylation using Endo H, albeit without obtaining the desired improvement in diffraction quality. Nonetheless, we found that optimization of the cryoprotection protocol based on incremental adjustments of the cryoprotecting solution to a final 20%(*v*/*v*) glycerol consistently gave better results. We therefore embarked on a large-scale screening of crystals, which resulted in a complete data set to 7.8 Å resolution (Fig. 3*c*, Table 1).

3.2.2. $Flt3_{D1–D4}$–FL complex. Initial crystallization experiments identified numerous hits for the $Flt3_{D1–D4}$–FL complex. By analogy to the crystallization-condition consensus for the $Flt3_{D1–D5}$–FL complex, these conditions were based on a medium-molecular-weight PEG and 0.1–0.2 *M* salt at pH 6–8.5. Based on crystal morphology arguments (overall crystal size, crystal thickness in the third dimension, singleness), a dozen conditions were selected for optimization. Diffraction experiments indicated 11–13%(*w*/*v*) PEG 4000, 100 m*M* $MgCl_2$, 50 m*M* MES pH 6.0 to be the most promising condition. Rod-like crystals appeared after 2–3 d and reached their final dimensions within 10 d. They grew as single rods measuring 0.3 × 0.1 × 0.02–0.05 mm (Figs. 4*a* and 4*b*) or as clusters that could easily be separated by manual intervention. $Flt3_{D1–D4}$–FL crystals generally diffracted to Bragg spacings of 5–4.5 Å. In contrast to the broad crystallization propensity of the $GlcNac_2Man_5$-glycosylated complex, we were not able to obtain crystals of the complex after treatment with EndoH, which is consistent with the notion that the extent of glycosylation is

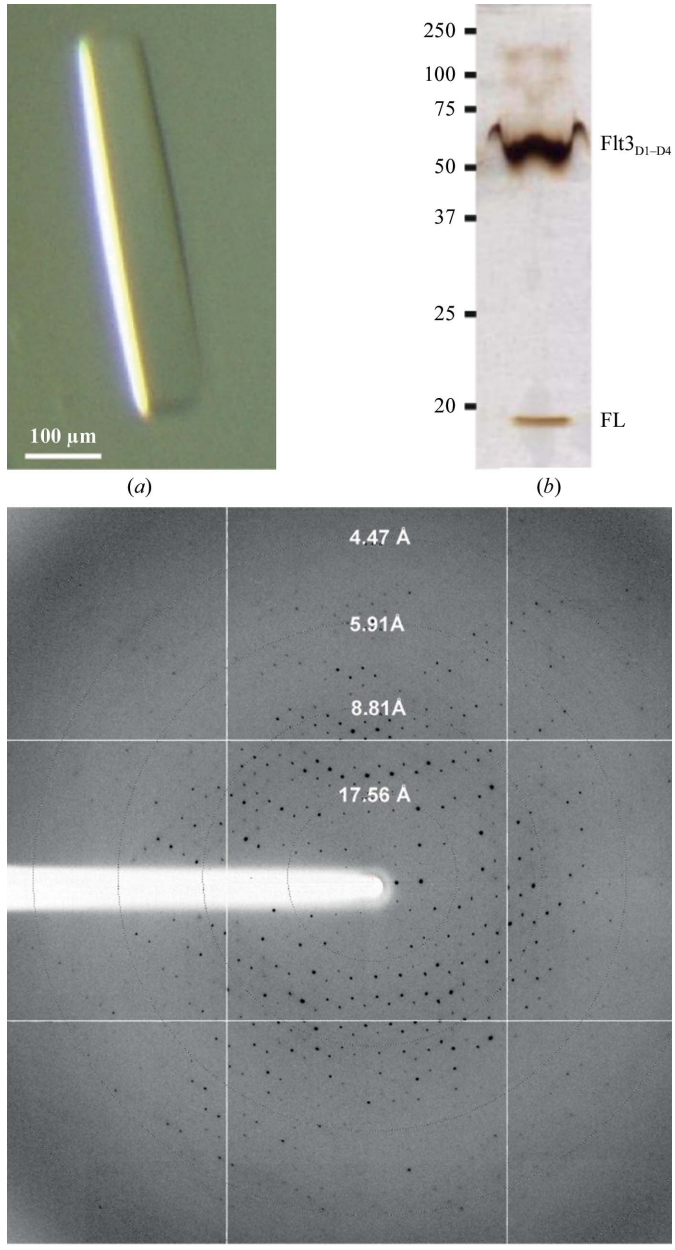

Figure 4
(*a*) Rod-like crystals of the $Flt3_{D1–D4}$–FL complex. (*b*) Silver-stained SDS–PAGE gel confirming the content of dissolved crystals of the $Flt3_{D1–D4}$–FL complex. (*c*) X-ray diffraction image from the $Flt3_{D1–D4}$–FL crystal that led to a complete data set to 4.3 Å resolution.

often not a strong predictor of crystallization behaviour (Mesters & Hilgenfeld, 2007). A recurring phenomenon during the course of crystal screening and characterization was a dramatic variation in diffraction quality and susceptibility to radiation damage even within the same crystal. Thus, we were unable to successfully employ data-collection strategies based on collecting partial data sets by systematically irradiating different parts of the crystal followed by merging of the resulting data. Cryoprotection of $Flt3_{D1–D4}$–FL crystals with 20% PEG 400 combined with a stochastic approach to crystal screening resulted in a final data set to 4.3 Å resolution (Fig. 4*c*, Table 1).

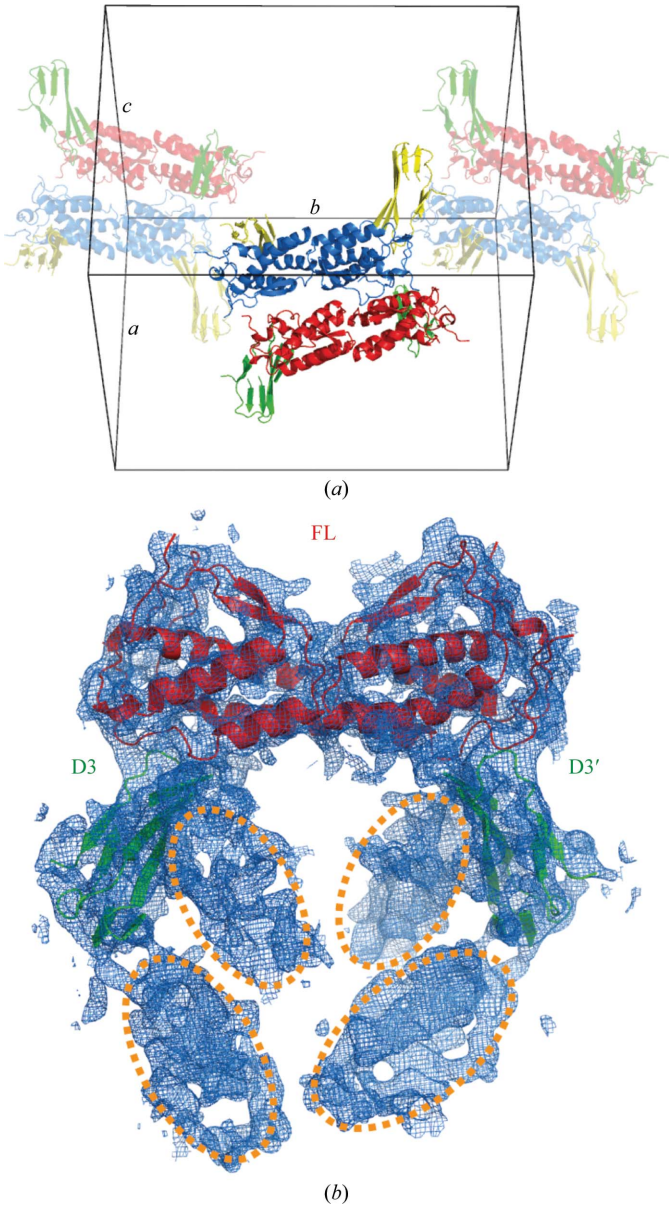

Figure 5
(*a*) Partial molecular-replacement solution for the $Flt3_{D1–D4}$–FL complex showing the presence of two complexes in the crystal asymmetric unit. Two neighbouring symmetry mates along the *b* axis are shown with appropriate depth cueing. FL (red and blue) and the MR model for $Flt3_{D3}$ (green and yellow) are shown in ribbon representation. (*b*) A density-modified electron-density map (contoured at 1σ) showing clear and complete electron density for unmodelled Flt3 extracellular domains (dashed ellipses). The map is the result of phase-improvement protocols implemented in the program *Parrot* based on the partial model obtained by MR using an NCS masking radius of 15 Å and 20 cycles of NCS averaging and solvent flattening. FL (red) and the MR model for $Flt3_{D3}$ (green) are shown in ribbon representation.

3.3. Structure determination of $Flt3_{D1–D4}$–FL

Owing to the superior diffraction quality of the $Flt3_{D1–D4}$–FL crystals, we focused our efforts on structure determination of the $Flt3_{D1–D4}$–FL complex. Phasing information for the crystal structure of $Flt3_{D1–D4}$–FL was initially determined at 4.3 Å resolution by maximum-likelihood molecular replacement (MR) as implemented in *Phaser* (McCoy *et al.*, 2007) using the structure of human FL (PDB entry 1ete; Savvides *et al.*, 2000) and a homology model for $Flt3_{D3}$ based on the structure of human KIT (PDB entry 2e9w; Yuzawa *et al.*, 2007). This revealed the presence of two $Flt3_{D1–D4}$–FL complexes in the crystal asymmetric unit that packed against each other *via* a broad interface between the two FL ligands (Fig. 5*a*). This packing arrangement was consistent with all major peaks in the self-rotation function as calculated with *MOLREP* (Vagin & Teplyakov, 2010). Furthermore, the corresponding electron-density map revealed a clear protein–solvent boundary for the two $Flt3_{D1–D4}$–FL complexes in the asymmetric unit, but was not of sufficient quality to allow model building. In our efforts to obtain additional experimental phase information we were confronted with the prohibitively poor diffracting capacity of $Flt3_{D1–D4}$–FL crystals derivatized with heavy atoms or selenomethionine-labelled $Flt3_{D1–D4}$. We therefore sought to improve the phase quality *via* density-modification approaches exploiting the presence of improper fourfold non-crystallographic symmetry (NCS) and the high solvent content of the crystals (59%). Such approaches have been sparsely applied to structure determinations *via* molecular replacement owing to possible limitations and phase bias imposed by the unimodal phase distribution inherent to calculated phases from protein models. However, when carefully applied, density modification based on initial phases calculated from partial molecular-replacement models can be very effective for both high- and low-resolution analyses (Huyton *et al.*, 2007; Keller *et al.*, 2006). Indeed, density-modification protocols as implemented in the program *Parrot* (Cowtan, 2010) starting with Hendrickson–Lattman coefficients for the phase probability distribution calculated in *Phaser* based on our initial molecular-replacement solution (covering only about 40% of the scattering mass in the asymmetric unit) revealed contiguous density for several unmodelled Flt3 domains including direct evidence for N-linked glycans (Fig. 5*b*). We note that extending the NCS mask radius parameter in *Parrot* from its default value of 6 to 15–20 was crucial for maximizing the quality of the electron-density maps and coverage of the asymmetric unit contents. We subsequently used the dramatically improved electron-density maps to select the correct MR solution for a homology model of $Flt3_{D4}$ based on KIT_{D4} and to manually place a model for $Flt3_{D2}$ based on KIT_{D5}. Model (re)building and refinement, including modelling of the elusive $Flt3_{D1}$ into electron density, are under way and will be reported elsewhere. The crystallized $Flt3_{D1–D4}$–FL and $Flt3_{D1–D5}$–FL complexes undoubtedly constitute a major milestone towards elucidating the overall architecture and organization of the extracellular Flt3–FL assembly, as well as towards gaining insights into the main features of the interaction epitope. We are currently working to develop shorter receptor constructs in light of the structural insights obtained from the $Flt3_{D1–D4}$–FL and $Flt3_{D1–D5}$–FL complexes in an effort to obtain crystals that will allow a detailed dissection of the receptor–ligand interface to high resolution.

KV, JE and KVC were supported by research fellowships from the Research Foundation Flanders, Belgium (FWO) and BR was

supported by the IWT-Flanders, Belgium. SNS is supported by the FWO (Projects 3G064307 and G059710) and Ghent University (BOF instrument). We would like to thank Isabelle Vandenberghe (L-Probe, Unit for Mass Spectrometry and Proteomics) for N-terminal sequence analysis. We thank the European Synchrotron Radiation Facility (ESRF) and the Swiss Light Source (SLS) for synchrotron beam time allocation, and the staff of beamlines ID-23 (ESRF), and X06SA/X06DA (SLS) for technical support. Access to these synchrotron facilities is supported by the European Commission under the 7th Framework Programme: Research Infrastructures, Grant Agreement Number 226716.

References

Aricescu, A. R., Lu, W. & Jones, E. Y. (2006). *Acta Cryst.* D**62**, 1243–1250.
Barash, S., Wang, W. & Shi, Y. (2002). *Biochem. Biophys. Res. Commun.* **294**, 835–842.
Chang, V. T., Crispin, M., Aricescu, A. R., Harvey, D. J., Nettleship, J. E., Fennelly, J. A., Yu, C., Boles, K. S., Evans, E. J., Stuart, D. I., Dwek, R. A., Jones, E. Y., Owens, R. J. & Davis, S. J. (2007). *Structure*, **15**, 267–273.
Cowtan, K. (2010). *Acta Cryst.* D**66**, 470–478.
Drexler, H. G. & Quentmeier, H. (2004). *Growth Factors*, **22**, 71–73.
Eklund, E. A. (2010). *Curr. Opin. Hematol.* **17**, 75–78.
Escobar, S., Brasel, K., Anderberg, R. & Lyman, S. (1995). *Blood*, **86**, 21a.
Fong, L., Hou, Y., Rivas, A., Benike, C., Yuen, A., Fisher, G. A., Davis, M. M. & Engleman, E. G. (2001). *Proc. Natl Acad. Sci. USA*, **98**, 8809–8814.
Grassot, J., Gouy, M., Perrière, G. & Mouchiroud, G. (2006). *Mol. Biol. Evol.* **23**, 1232–1241.
Griffith, J., Black, J., Faerman, C., Swenson, L., Wynn, M., Lu, F., Lippke, J. & Saxena, K. (2004). *Mol. Cell*, **13**, 169–178.
Hannum, C., Culpepper, J., Campbell, D., McClanahan, T., Zurawski, S., Bazan, J. F., Kastelein, R., Hudak, S., Wagner, J. & Mattson, J. (1994). *Nature (London)*, **368**, 643–648.
Heras, B. & Martin, J. L. (2005). *Acta Cryst.* D**61**, 1173–1180.
Huyton, T., Zhang, J.-G., Luo, C. S., Lou, M.-Z., Hilton, D. J., Nicola, N. A. & Garrett, T. P. (2007). *Proc. Natl Acad. Sci. USA*, **104**, 12737–12742.
Kabsch, W. (2010). *Acta Cryst.* D**66**, 125–132.
Kantardjieff, K. A. & Rupp, B. (2003). *Protein Sci.* **12**, 1865–1871.
Keller, S., Pojer, F., Heide, L. & Lawson, D. M. (2006). *Acta Cryst.* D**62**, 1564–1570.
Kikushige, Y., Yoshimoto, G., Miyamoto, T., Iino, T., Mori, Y., Iwasaki, H., Niiro, H., Takenaka, K., Nagafuji, K., Harada, M., Ishikawa, F. & Akashi, K. (2008). *J. Immunol.* **180**, 7358–7367.
Kindler, T., Lipka, D. B. & Fischer, T. (2010). *Blood*, **116**, 5089–5102.
Kiyoi, H. & Naoe, T. (2006). *Int. J. Hematol.* **83**, 301–308.
Kiyoi, H., Ohno, R., Ueda, R., Saito, H. & Naoe, T. (2002). *Oncogene*, **21**, 2555–2563.
Kiyoi, H., Towatari, M., Yokota, S., Hamaguchi, M., Ohno, R., Saito, H. & Naoe, T. (1998). *Leukemia*, **12**, 1333–1337.
Lavagna, C., Marchetto, S., Birnbaum, D. & Rosnet, O. (1995). *J. Biol. Chem.* **270**, 3165–3171.
Liu, K. & Nussenzweig, M. C. (2010). *Immunol. Rev.* **234**, 45–54.
Lyman, S. D. *et al.* (1993). *Cell*, **75**, 1157–1167.
Lyman, S. D., James, L., Escobar, S., Downey, H., De Vries, P., Brasel, K., Stocking, K., Beckmann, M. P., Copeland, N. G. & Cleveland, L. S. (1995). *Oncogene*, **10**, 149–157.
Lyman, S. D., James, L., Zappone, J., Sleath, P. R., Beckmann, M. P. & Bird, T. (1993). *Oncogene*, **8**, 815–822.
Maroc, N., Rottapel, R., Rosnet, O., Marchetto, S., Lavezzi, C., Mannoni, P., Birnbaum, D. & Dubreuil, P. (1993). *Oncogene*, **8**, 909–918.
Matthews, B. W. (1968). *J. Mol. Biol.* **33**, 491–497.
McClanahan, T., Culpepper, J., Campbell, D., Wagner, J., Franz-Bacon, K., Mattson, J., Tsai, S., Luh, J., Guimaraes, M. J., Mattei, M. G., Rosnet, O., Birnbaum, D. & Hannum, C. H. (1996). *Blood*, **88**, 3371–3382.
McCoy, A. J., Grosse-Kunstleve, R. W., Adams, P. D., Winn, M. D., Storoni, L. C. & Read, R. J. (2007). *J. Appl. Cryst.* **40**, 658–674.
Mesters, J. R. & Hilgenfeld, R. (2007). *Cryst. Growth Des.* **7**, 2251–2253.
Monneret, C. (2005). *Eur. J. Med. Chem.* **40**, 1–13.
Onai, N., Obata-Onai, A., Schmid, M. A., Ohteki, T., Jarrossay, D. & Manz, M. G. (2007). *Nature Immunol.* **8**, 1207–1216.
Parcells, B. W., Ikeda, A. K., Simms-Waldrip, T., Moore, T. B. & Sakamoto, K. M. (2006). *Stem Cells*, **24**, 1174–1184.
Reeves, P. J., Callewaert, N., Contreras, R. & Khorana, H. G. (2002). *Proc. Natl Acad. Sci. USA*, **99**, 13419–13424.
Savvides, S. N., Boone, T. & Karplus, P. A. (2000). *Nature Struct. Biol.* **7**, 486–491.
Schmid, M. A., Kingston, D., Boddupalli, S. & Manz, M. G. (2010). *Immunol. Rev.* **234**, 32–44.
Stein, N. (2008). *J. Appl. Cryst.* **41**, 641–643.
Stirewalt, D. L. & Radich, J. P. (2003). *Nature Rev. Cancer*, **3**, 650–665.
Vagin, A. & Teplyakov, A. (2010). *Acta Cryst.* D**66**, 22–25.
Verstraete, K., Koch, S., Ertugrul, S., Vandenberghe, I., Aerts, M., Vandriessche, G., Thiede, C. & Savvides, S. N. (2009). *Protein J.* **28**, 57–65.
Waskow, C., Liu, K., Darrasse-Jèze, G., Guermonprez, P., Ginhoux, F., Merad, M., Shengelia, T., Yao, K. & Nussenzweig, M. (2008). *Nature Immunol.* **9**, 676–683.
Yao, F., Svensjö, T., Winkler, T., Lu, M., Eriksson, C. & Eriksson, E. (1998). *Hum. Gene Ther.* **9**, 1939–1950.
Yuzawa, S., Opatowsky, Y., Zhang, Z., Mandiyan, V., Lax, I. & Schlessinger, J. (2007). *Cell*, **130**, 323–334.
Zheng, R., Levis, M., Piloto, O., Brown, P., Baldwin, B. R., Gorin, N. C., Beran, M., Zhu, Z., Ludwig, D., Hicklin, D., Witte, L., Li, Y. & Small, D. (2004). *Blood*, **103**, 267–274.